Electronic Supplementary Material (ESI) for Nanoscale.
This journal is © The Royal Society of Chemistry 2020

Supplementary Information for "Quantitative measurement of charge accumulation along a quasi-one-dimensional W_5O_{14} nanowire during electron field emission"

Fengshan Zheng,[*,†] Giulio Pozzi,[†,‡] Vadim Migunov,[†,¶] Luka Pirker,[§] Maja Remskar,[§] Marco Beleggia,[‖] and Rafal E. Dunin-Borkowski[†]

†*Ernst Ruska-Centre for Microscopy and Spectroscopy with Electrons and Peter Grünberg Institute, Forschungszentrum Jülich, 52425 Jülich, Germany*

‡*Department of Physics and Astronomy, University of Bologna, Viale Berti Pichat 6/2, 40127 Bologna, Italy*

¶*Central Facility for Electron Microscopy (GFE), RWTH Aachen University, Ahornstrasse 55, 52074 Aachen, Germany*

§*Jozef Stefan Institute, Solid-State Physics Department, Jamova 39, SLO-1000 Ljubljana, Slovenia*

‖*DTU Nanolab, Technical University of Denmark, 2800 Kgs. Lyngby, Denmark*

E-mail: f.zheng@fz-juelich.de

Representative off-axis electron hologram

Fig. 1 shows a representative off-axis electron hologram recorded with the W_5O_{14} nanowire at an applied bias voltage of 150 V. The interference fringe spacing was 2.4 nm (5.4 pixels), resulting in a spatial resolution of approximately 5 nm in reconstructed phase images. The width of the interference region was approximately 2 μm. The inset shows a magnified view of the interference fringes around the apex region. This nanowire was contaminated slightly by an approximately 10-nm-thick amorphous layer.

The surface contamination layer is thought to result from a combination of specimen preparation, exposure to air before TEM examination and electron beam illumination in the high vacuum environment of the TEM column. We did not observe any change in this surface layer with time or electron fluency. In the future, it would be beneficial to reduce the presence of such contamination layers by using an ultra high vacuum TEM column, as well as either inert sample transfer or combined sample preparation and characterization in the same instrument.

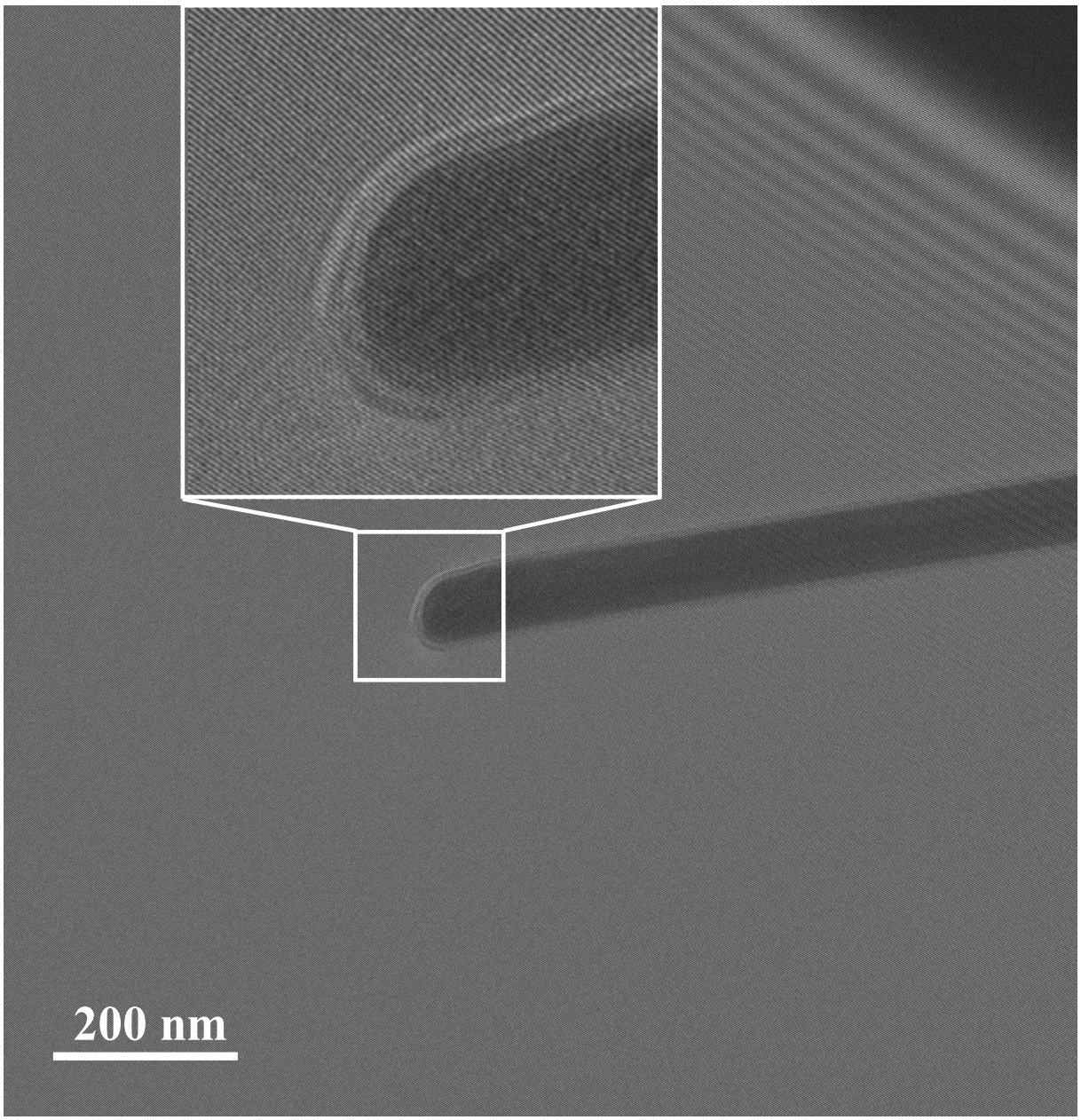

Figure 1: Representative off-axis electron hologram of the W_5O_{14} nanowire at an applied bias voltage of 150 V. The inset shows a magnified view of the interference fringes around the apex region. An approximately 10-nm-thick amorphous layer is visible on the surface of the nanowire.

Mean inner potential contribution to the phase

As a result of the fact that a strong electrostatic force acts on the nanowire when it is subjected to a high electrical bias, it is observed to bend. The alignment of phase images to calculate differences between results recorded at different applied bias voltages, in order to subtract the mean inner potential (MIP) contribution to the phase, is then difficult or impossible. Therefore, the analyses presented in this paper were performed without subtracting the MIP contribution to the phase, resulting in the possibility of artefacts in subsequent charge density measurements.[S1] The influence of the MIP contribution to the phase on charge density measurements is considered below.

Fig. 2a shows a phase image acquired in the absence of an applied bias voltage, *i.e.*, comprising only the MIP contribution. Such an image is directly proportional to the projected thickness of the nanowire (in the absence of dynamical diffraction). It can be used to determine the influence of the MIP contribution to the phase on the calculated charge density. A line profile extracted from the phase image across the nanowire axis (marked by a magenta line in Fig. 2a) suggests that it has a quasi-rectangular cross-section (Fig. 2c, magenta). A second line profile extracted along the nanowire axis (marked by a green line in Fig. 2a) indicates that the nanowire has a sharply terminated thickness profile at its apex (Fig. 2c, green), with a transition distance that is not greater than 15 nm, including the 10-nm-thick amorphous layer. The flatness of the phase in the vacuum region in both phase profiles confirms that the unbiased nanowire is not significantly charged electrically in the presence of the high-energy electron beam.

Additional contributions to the charge density arising solely from the MIP contribution to the phase can result from gradients in phase at the edge of the object, where its projected thickness is changing. Such "artificial" or effective charges are visible in Figs. 2d-e, which show cumulative charge profiles integrated along the dashed rectangle marked in Fig. 2a from the base to the apex (red arrow) and from one edge to the other (blue arrow), respectively. The *total* effective charge associated with the MIP contribution to the phase is zero in both

cases. Therefore, measurements of the *total* charge are likely to be free of artefacts, even in the presence of the MIP contribution to the phase. For integration along the nanowire axis, as indicated by the red arrow in Fig. 2a and by Fig. 2d, the cumulative charge is always zero except when the integration region approaches the apex of the nanowire. The fact that the cumulative charge profile is negative and then returns to zero is consistent with the Laplacian of the MIP contribution to the phase shown in Fig. 2b. As the "artificial" charges due to the MIP contribution to the phase are present in a narrow (15 nm) region at the apex of the nanowire, this region was excluded from the analysis (*i.e.*, the fitting of the profiles) presented in the main text.

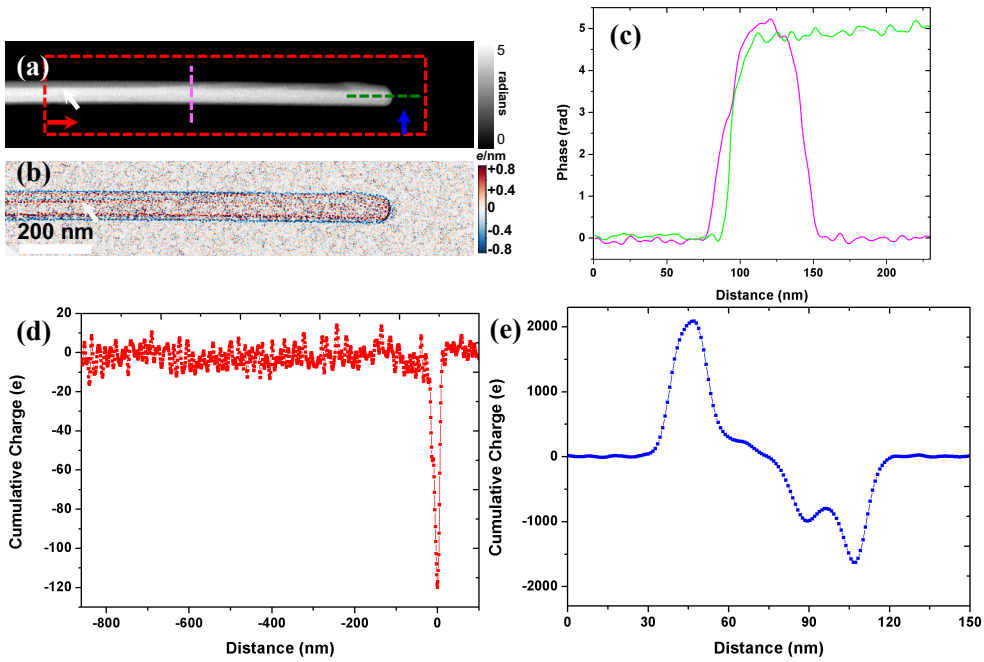

Figure 2: The MIP contribution to the phase alone and its effect on the measurement of cumulative charge profiles: (a) Phase image recorded without an applied electrical bias, *i.e.*, corresponding to the MIP contribution only. (b) Effective charge density calculated from the Laplacian of (a) using Eq. 2 in the main text. (c) Phase profiles extracted from (a) along the nanowire axis (green) and across the nanowire axis (magenta). (d) and (e) Cumulative charge profiles measured from (b) along the nanowire axis and across the nanowire axis, respectively, from the region marked by a red dashed rectangle in (a). The integration region was allowed to shrink in the direction of the red/blue arrow to create the line profiles shown in (d) and (e), respectively.

Model of the charge density and fit of the cumulative charge

In order to find a suitable analytical function describing the accumulation of the charge at the tip of our nanowire, we elaborate an important suggestion in the paper by Griffiths and Li,[S2] who were in turn inspired by the treatment by Smythe[S3] of a finite cylinder. They considered the so-called "fundamental term" in Smythe's series expansion of the charge density along a cylinder of length $2A_0$, oriented with its axis parallel to the y axis, which takes the form

$$\lambda(y_0) = C_0 + \frac{B_0}{(A_0^2 - y_0^2)^{1/3}}. \tag{S1}$$

In this way, they obtained an excellent agreement with their discrete charge distribution.

In the present study, it is of interest to determine what happens at the apex of the nanowire, say for $y_0 \leq A_0$. By assuming that A_0 is large, we obtain the following model for the charge distribution

$$\lambda(y_0) = C_0 + \frac{B}{(A_0 - y_0)^{1/3}}, \tag{S2}$$

where $B = \frac{B_0}{(2A_0)^{1/3}}$.

In order to reproduce our data, we also introduce a linear term. Renaming the parameters, we obtain the expression

$$\lambda(y_0) = C_0 + \frac{B}{(A_0 - y_0)^{1/3}} + Dy_0. \tag{S3}$$

In our experiments, the field of view is limited and only a finite length of the nanowire can be seen. If the length inside the field of view is A, then y_0 in this coordinate system varies from $(A_0 - A)$ to A_0. As the origin of the above coordinate system cannot be determined in the experimental data, we allow y to start from 0 at the left edge of the image and to end

at the right edge of the image, *i.e.*, $y = y_0 - (A_0 - A)$. In this coordinate system, Eq. S3 can be reduced to the form

$$\lambda(y) = C + \frac{B}{(A-y)^{1/3}} + Dy, \tag{S4}$$

where $C = C_0 + D(A_0 - A)$.

By integrating the above expression to find the cumulative charge and imposing the restriction that the cumulative charge must be zero at the tip and beyond, we finally obtain the expression for the cumulative charge

$$-\frac{1}{2}A(2C + AD) + Cy + \frac{1}{2}Dy^2 - \frac{3}{2}B(A-y)^{2/3}. \tag{S5}$$

This function provides excellent fits to our experimental data, as shown in Fig. 3 and Table 1).

Table 1: Fitted parameters to experimental cumulative charge profiles for different applied bias voltages, based on Eq. S5.

Voltage(V)	A	B	C	D
130	746.22	42.11	2.60	-4.83×10^{-4}
140	746.76	45.21	2.85	-5.72×10^{-4}
150	746.27	49.02	2.91	-4.75×10^{-4}
160	746.24	53.24	3.04	-6.77×10^{-4}
170	746.12	56.94	3.133	-1.10×10^{-3}
180	746.33	60.51	3.40	-9.95×10^{-4}
182	746.95	60.62	3.58	-1.00×10^{-3}
184	748.24	62.68	3.78	-9.46×10^{-4}
186	747.53	61.26	3.58	-6.29×10^{-4}

Although the goodness of fit provides strong evidence that the accumulation of charge at the apex of the nanowire can be described successfully using Eq. S5, the parameters cannot be determined for the whole nanowire, but only for its apex. In order to obtain this information in a more general way and to assess the relative weights of the linear and additional "accumulation" contributions to the field enhancement factor, we now consider the more idealised geometry of a line charge distribution in the presence of a flat anode.

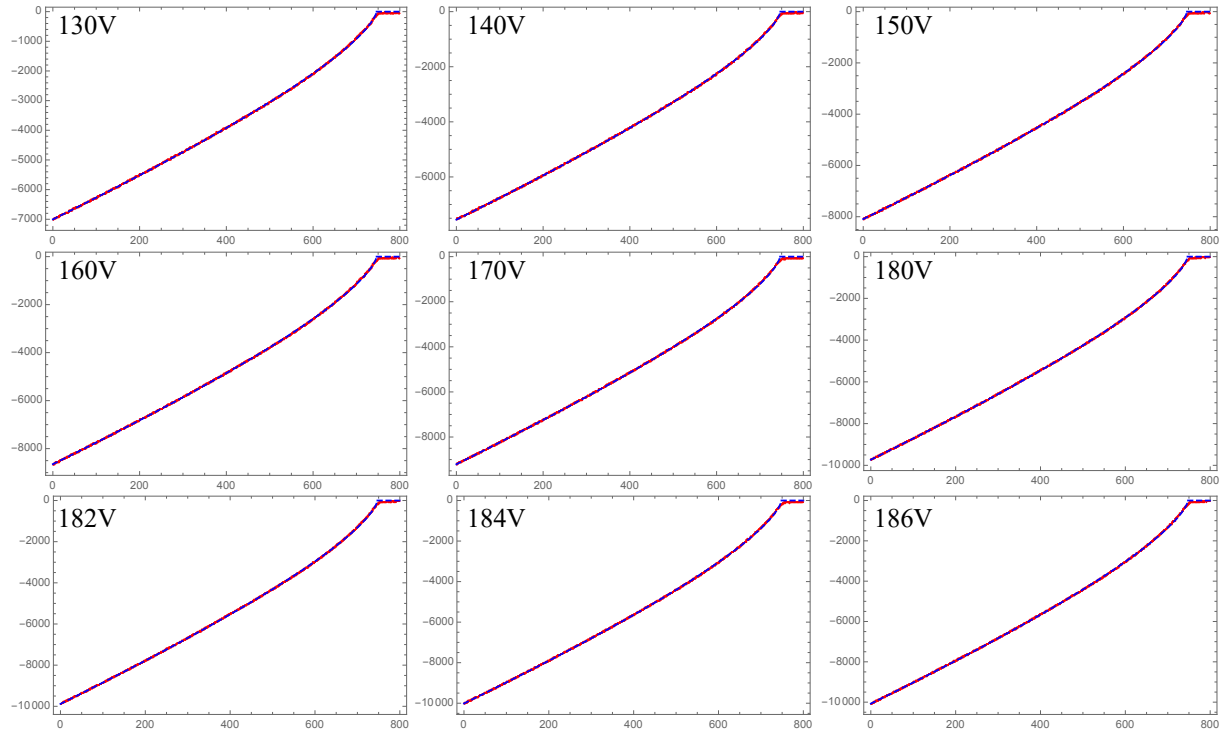

Figure 3: Fitting of experimental cumulative charge profiles at different bias voltages based on Eq. S5. The number in the upper left of each image denotes the applied bias voltage. The experimental data are shown in dashed black lines and the fits are shown in red. The horizontal axis in each image is distance (nm), while the vertical axis in each image is cumulative charge (electrons).

Rounded cylindrical needle on a conducting plane

As shown by Durand[S4] (see also the work of Pogorelov and co-workers[S5]), we consider the case of a line charge of length A_0, protruding perpendicularly from a conducting plane along the y direction in the presence of an applied constant field E_0 (*i.e.*, a linear electrostatic potential $-yE_0$) and having a linear charge density distribution vanishing on the plane. If we add the image charges with respect to the plane, at $V = 0$, it turns out that the equipotential surface at $V = 0$ outside the plane corresponds to the shape of a hemi-ellipsoid and is able to represent a metallic hemi-ellipsoidal emitter on a plate in a constant field. Points $(0, -A_0)$ and $(0, A_0)$ are the foci of the ellipse. At a fixed field, let us take it unity for convenience, and fixed length A_0, the coefficient of the linear density of charge is in one to one relationship with the shape of the ellipse. So, if we choose the radius R at the base of the hemi-ellipsoid

at $y = 0$, also the charge density is fixed as well as the potential and field in the whole space.

Here, we apply the same procedure to investigate the addition to a linear charge distribution of Smythe's fundamental term (Eq. S4), noting that this extra parameter introduces a new degree of freedom which is able to affect the shape of the emitter. With the condition that $\lambda(0) = 0$, *i.e.*, line charge distribution for $y \geq 0$ becomes

$$\lambda(y) = -B + \frac{B}{(1-y)^{1/3}} + Dy. \tag{S6}$$

.

A more intuitive physical meaning can be ascribed to the parameters by expressing them as a function of the total charge in the linear term q_{lin} and the total charge in the nonlinear term q_{tip}, resulting in the expression

$$\lambda(y) = -2\frac{q_{tip}}{A} + 2\frac{q_{tip}}{A^{2/3}(A-y)^{1/3}} + 2q_{lin}\frac{y}{A^2}. \tag{S7}$$

.

For $y \leq 0$, an image charge distribution should be added to keep the plane $y = 0$ at zero potential. The potential in the entire space then takes the form

$$V(r,y) = \int_0^A \frac{1}{4\pi\epsilon_0}\left(\frac{1}{\sqrt{(t-y)^2+r^2}} - \frac{1}{\sqrt{(t+y)^2+r^2}}\right)\lambda(t)dt - y, \tag{S8}$$

where $r = \sqrt{x^2+z^2}$ is the radial coordinate, the second term in the brackets corresponds to the image charge and the linear term y corresponds to an added electric field of unit intensity. Softwares such as Mathematica[S6] can be used to provide an analytical solution to this integral equation in terms of hypergeometric confluent functions. However, it is more convenient to evaluate it numerically. By defining $k = \frac{q_{lin}}{q_{tip}}$ and setting the radius at the base (in practice at a small distance from the equipotential plane) to be equal to the radius of the needle, the last free parameter is used to define the zero equipotential and hence the shape of the emitter. The electric field E can be obtained by taking the gradient of Eq. S8.

Fig. 4 shows the dependence of the shape of the tip of the nanowire for $A_0 = 9.4$ μm and $R = 40$ nm, which are close to the experimental values of our nanowire. Fig. 4a represent the case for $q_{lin} = 1$ and $q_{tip} = 1$, Fig. 4b for $q_{lin} = 5$ and $q_{tip} = 1$ and Fig. 4c for $q_{lin} = 10$ and $q_{tip} = 1$. Owing to the very large aspect ratio we have shown only the region over 1 μm around the tip (distances are in μm). We can see that in the first case (a), with the relatively predominant Smythe term, the shape of the wire is larger at the tip that at the base. In the second case (b) the shape become more cylindrical whereas in the case (c), with predominant linear term, the shape turns into that of an elongated ellipsoid.

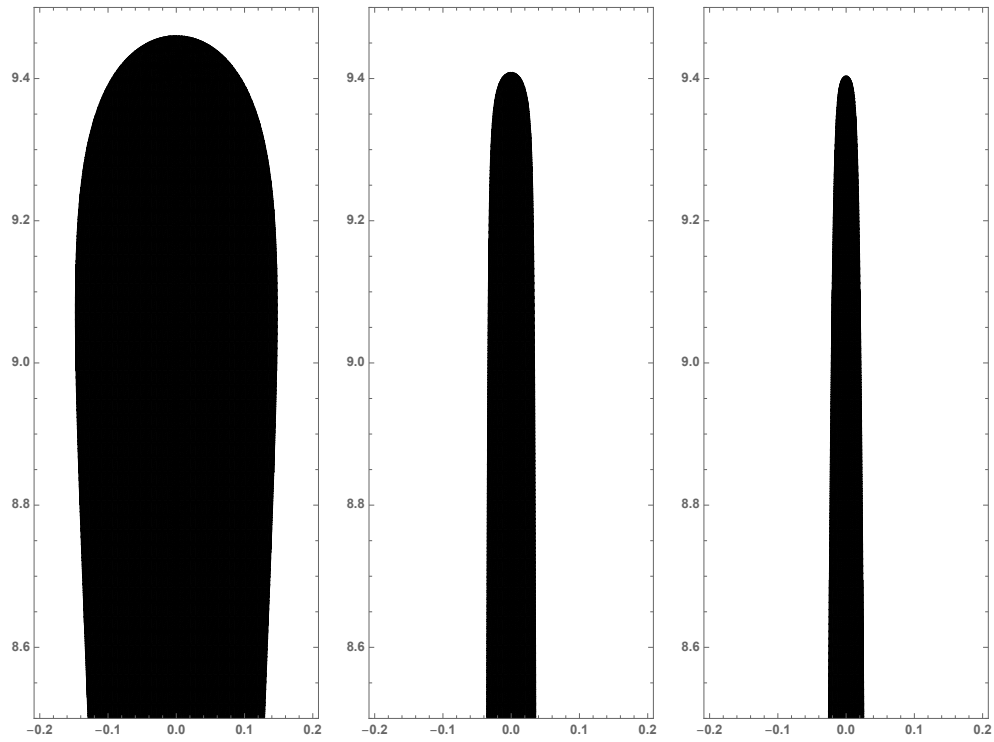

Figure 4: Shape of the nanowire near the tip for (a) $q_{lin} = 1$ and $q_{tip} = 1$, (b) $q_{lin} = 5$ and $q_{tip} = 1$ and (c) $q_{lin} = 10$ and $q_{tip} = 1$ in a region over 1 μm around the tip. Distances are shown in units of μm.

Luckily, we do not need more terms in the Smythe expansion[S3] for describing our rounded cylindrical nanowire. Having fixed the shape, we can proceed and numerically calculate the electric field in the space around the tip and at the tip itself, where is needed to calculate

current density according to the Fowler-Nordheim expression.[S7]

$$j = \frac{C_1 E^2}{\phi} \exp\left(-\frac{C_2 \phi^{3/2}}{E}\right), \tag{S9}$$

where $\phi = 4.3$ eV[S8] is the work function of W_5O_{14} and the first and second Fowler-Nordheim constants are $C_1 = 1.56 \times 10^{-6}$ A eV V^{-2} and $C_2 = 6.83 \times 10^9$ eV$^{-3/2}$ V m^{-1}, respectively. Note that if the work function were to be significantly affected by the surface contamination layer, then a space charge region could form at the wire/contamination layer interface. While we cannot rule out such effects, they are below the sensitivity of the present measurements and require a separate higher spatial resolution study.

By numerically integrating this expression over the surface of the apex, it is possible to calculate the emission current. In the main text, Fig. 5, are reported the results of the calculations for the electric field around the tip, on the axis from the tip and of the emission current for the values of $k = 4$, 5 and 6. It is reassuring that a satisfying agreement with the experimental data is obtained for $k = 5$.

Field emission

The observed fluctuation in field emission current may result from the fact that the emitted electrons are not all collected by the counter-electrode, but instead collide with gas atoms in the TEM column, travel far from the counter-electrode, or are attracted by positively ionised particles. Another possible reason is that the surface of the nanowire may change slightly during field emission, either due to contamination from gas atoms in the column or as a result of the fly-out of surface atoms, *e.g.*, from the amorphous layer. Note that the amorphous layer changed little before or after field emission experiments.

The stop in emission at 188 V may indicate that the distance between the nanowire and the counter-electrode became larger due to an instability in the movable hat, that the surface of the nanowire changed dramatically, that the field-emitted electrons created ions at the

counter-electrode that were attracted by the nanowire, or that the nanowire became shorter due to field emission or the heating current.

Between 148 V and 180 V, the measurements follow a linear relationship between $\frac{1}{V}$ and $\ln \frac{I}{V^2}$, which can be expressed after linear fitting in the form

$$\ln \frac{I}{V^2} = -1842.73 \frac{1}{V} - 17.46. \tag{S10}$$

The slope of the *F-N* plot is linked directly to the field enhancement factor and the work function[S9] as follows:

$$1842.73 = \frac{C_2 \phi^{1.5} d_{capacitor}}{\gamma}, \tag{S11}$$

where $d_{capacitor}$ is the distance between the two large plates, *i.e.*, the counter-electrode and the micro-sized W wire (the support) onto which the nanowire is attached and γ is the field enhancement factor. As the distance was 10.5 μm (see Fig. 1 in the main text), the field enhancement factor could be estimated to be approximately 347. On the assumption of an onset voltage for field emission of 148 V, the local electric field could then be calculated to be $E_{loc} = \gamma \frac{V}{d_{capacitor}} = 4.90$ V/nm.

References

[S1] Zheng, F.; Caron, J.; Migunov, V.; Beleggia, M.; Pozzi, G.; Dunin-Borkowski, R. E. *Journal of Electron Spectroscopy and Related Phenomena* **2020**, in press.

[S2] Griffiths, D. J.; Li, Y. *American Journal of Physics* **1996**, *64*, 706–714.

[S3] Smythe, W. *Journal of Applied Physics* **1956**, *27*, 917–920.

[S4] Durand, E. *Électrostatique*; Masson: Paris, 1964; Vol. 2.

[S5] Pogorelov, E. G.; Zhbanov, A. I.; Chang, Y.-C. *Ultramicroscopy* **2009**, *109*, 373–378.

[S6] Wolfram, S. *The Mathematica book*, 4th ed.; Wolfram Media: Champaign, IL, 1999.

[S7] Fowler, R. H.; Nordheim, L. *Proc. R. Soc. Lond. A* **1928**, *119*, 173–181.

[S8] Ulisse, G.; Ciceroni, C.; Carlo, A.; Brunetti, F.; Jelenc, J.; Saqib, M.; Varlec, A.; Remskar, M. *Microelectronic Engineering* **2017**, *170*, 44 – 48.

[S9] Bonard, J.-M.; Croci, M.; Arfaoui, I.; Noury, O.; Sarangi, D.; Châtelain, A. *Diamond and Related Materials* **2002**, *11*, 763–768.